A comparison of feature extraction techniques for delamination of CFRP using ECPuCT system

X.Lu[1], Q. Yi[1*], G.Y. Tian[1,2]
[1]School of Engineering, Newcastle University, Newcastle Upon Tyne, UK
[2]University of Electronic Science and Technology of China

***Abstract*— CFRP (carbon fiber reinforced plastic) has replaced conventional metallic materials in many industrial applications because of its outstanding mechanical performance such as high strength to ratio and resistance of fatigue. During the serving life of the aerospace composite component, delamination left without detection can cause a sudden breakdown of the structure. Eddy current pulse-compression thermography (ECPuCT) is an emerging technique combines traditional ECPT and pulse compression techniques. In this work, feature extraction techniques of impulse response have been exploited in terms of principal component analysis (PCA), kernel principal component analysis (K-PCA) and independent component analysis (ICA) Each technique is evaluated using SNR as the index to compare the performance. The results indicate that Kernel-PCA performs better than PCA and ICA based features when dealing with delamination ranged from defect#1(0.46mm) to defect#9 (2.30mm).**

Keywords—CFRP; eddy current pulse-compression thermography; kernel-PCA; ICA; SNR

I. INTRODUCTION

Carbon fiber reinforced plastic as a kind of emerging composite material, has been used widely in many industrial applications, because of its remarkable performance such as high stiffness and low density. Thus, the integrity of CFRP under various loading conditions like impact loading is very critical for the structure. Delamination is one of the most common defects for CFRP, they mostly occur and grow between different layers of CFRP. The structure of CFRP with delamination has lower strength and stiffness, which may lead to the fragility of the overall structure [1]. Under these circumstances, regular quality testing of composite can eliminate potential hazards as far as possible [2].

Numerous Non-destructive testing (NDT) techniques were used in the CFRP delamination detection. For instance, the ultrasonic testing technique was applied in the detection of delamination, but its results are easily distorted by high frequency [3]. At present, the main NDT techniques for CFRP are ultrasonic testing, X-ray, eddy current, microwave, etc. However, those techniques have several drawbacks. Firstly, their systems are huge and complicated, such as the device of X-ray is complex, large, time-consuming, and the radiation is harmful to the human body, so inspectors need extra protection [4]. Secondly, low detection depth makes it is hard to find deep defects, such as laser speckle method is only suitable for detection of subsurface defects because of its detection based on the difference of sample deformation and the change of temperature field [5]. Thirdly, it is challenging to realize NDT for those methods, such as traditional ultrasonic detection. Fourthly, those methods cannot effectively suppress the influence of noise, which leads to low sensitivity and resolution of detection [3].

Active Thermography (AT) was proposed to detect delamination in CFRP, it makes up for the shortcomings of previous traditional NDT techniques. AT can achieve a large range of one-time detection, but also can be applied in various practical situations such as material characterization [6], structure monitoring. In AT, the thermal contrast is achieved through different external heating sources. Optical sources is a most common physical source [7], they generate heat on the sample surface and heat diffuses into the sample for thermal equilibrium. However, optically stimulated thermography (QST) or flush thermography may not suitable for detecting in-depth damage, closed cracks at the early stages [8]. Ultrasonic stimulated thermography (UST) is an alternative means of thermography that is mainly used for the inspection of micro-cracks in aluminium aerospace components [9] and composite primary and secondary structures [8]. The delamination detection of UST often suffered from problems of multi-layer and heterogeneous structures.

ECPT is an emerging NDT technique, it performs effectively than conventional NDT technique in the detection of CFRP defects [10]. Besides, it has higher detection efficiency and in-depth capability, higher resolution than traditional eddy current because of the combination of multi-physics nature which combines Joule heating and heat diffusion[11]. In ECPT system, a coil carried with high-frequency alternating current is used to excite eddy current inside the sample. The abnormal structure of surface and subsurface will change the distribution density of the eddy current, which leads to the irregularity of the thermal distribution observed by the infrared camera [12]. In previous works, the application of ECPT has been studied for detection and quantities of fatigue cracks, corrosion, and loading impact [13]. Since CFRP exhibits low electrical conductivity, the process can be considered volumetric heating because the skin depth of eddy-current is greater than the thickness of CFRP sample in most of the ECPT cases [14]. Therefore, the surface conditions of CFRP sample affect the results of ECPT. Besides, the complex structure of CFRP, such as multi-layer structure, anisotropic conductivity and different fibre orientation, leads to non-uniform thermal distribution. Based on those reasons, faithful quantitative evaluation of the delamination depth from thermal response was obstructed [14].

To improve the detection capability of ECPT, the combination of pulse-compression (PuC) techniques and eddy current excitation was proposed as ECPuCT in recent works [8,14]. It has been proven that PuC technique applied with AT ameliorates attainable Signal-to-Noise Ratio (SNR) even under low-power heat sources [15, 16]. At present works, ECPuCT can be successfully used in the detection and quantitative evaluation of delamination located in CFRP [14]. The ECPuCT applies a modulated current waveform to excite eddy current, the matched-filter is applied pixel-wise on time

trends to retrieve the impulse response of the sample as thermograms [14, 17].

Apart from the improvement of detectability of defects beyond the skin depth based on the ECPuCT method, feature extraction methods were applied in this work, which is critical for quantitative evaluation of defect depth. The features for ECPuCT system are presented by thermal distribution in thermal sequences and transient responses in time domain. For thermal sequences extraction, the main goal is to define the location of defect based on thermal images. Principal component analysis (PCA) was applied by transform the raw data into orthogonal principal component subspace, which also reduces the dimension of data [18]. Independent component analysis (ICA) was proposed to identify the significant ICs in the mixing observation model [19]. Single-channel blind source separation was proposed in [20], it enables spatial and time patterns to be extracted based on transient thermal response behaviour. Thermal transient response features have been applied to indicate the status of defect. Fourier transform was used for pulse thermography (PT), it has been proven that the non-uniform heating and surface emissivity variation was removed based on this method [21]. Wavelet transform was proposed which has the potential of automatically selecting both optimal transient frame and spatial scale for defect localization with ECPT system [22].

Since the distribution of the thermal transient response is Gaussian distribution, kernel function was introduced in PCA in previous work. Traditional PCA always find principal linear components to represent the data in lower dimension. For data with non-linear distribution, PCA will fail to find right representative direction. Kernel-PCA rectifies this limitation [14]. For the same reason, kernel-ICA was applied in this work for comparison of the performance of those feature extraction methods.

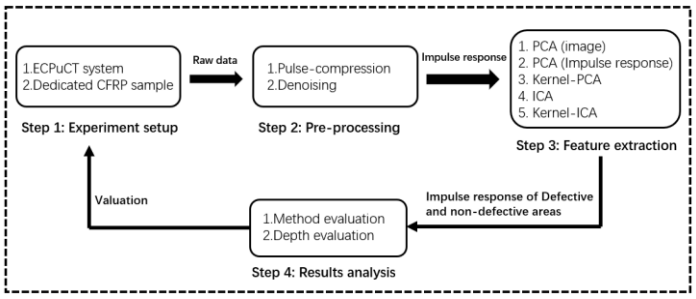

Figure 1 Systematic diagram

Figure 1 shows the block diagram of overall work based on the ECPuCT system. In the first stage, ECPuCT method was first applied to the CFRP sample with manual delamination located at different depth. Then the raw data, presented as thermal sequences, processed with denoising algorithm in order to remove noise. In the third stage, five different feature extraction algorithms exploited to localize the delamination defect and enhance the delamination area. Based on the results of feature extraction, SNR between defective area and non-defective area was exploited to compare the performance of those methods. SNR reflects the accuracy of feature extraction; SNR value curves reflect the performance of feature extraction method when dealing with different depth defects. If the SNR curve decreases slowly and keeps a stable value, the method is more reliable. Combined with physical meaning, the valuation of feature extraction methods is precise.

This paper is organized as follows: Section II introduces the theoretical background of ECPuCT system and feature extraction algorithms proposed. Section III presents details about the Backer code excitation, ECPuCT experimental setup, and the dedicated CFRP sample. Section IV discusses the results of feature extraction combined with physical meaning, and SNR comparison of their performance. The crossing-point feature validation of delamination depth also presented in this section. The conclusion will be made in section V.

II. PROPOSED METHODOLOGY

A. *Pulse-compression theory*

Pulse compression infrared thermography testing is a burgeoning technique that has been used widely in the experimental estimation of impulse response based on Linear Time Invariant (LTI) system, it is suitable for noisy experimental environment or experiment results with low SNR value [23]. The combination of pulse compression technology and infrared thermal imaging nondestructive testing technology can effectively improve the signal-to-noise ratio and thermal contrast of the results and enhance the detection effect. In standard ECPuCT system, heating time is significantly shorter than cooling time. Therefore, the so-provided heating stimulus can be modeled as a Dirac's Delta function $\delta(t)$, and the corresponding output $\mathrm{y}(t)$. The temperature response curve of each pixel in the collected data is consistent with the pulse thermal imaging mode. The defect information can be determined by analyzing the data of the heating stage and the cooling stage [24]. Features are obtained by analyzing the $\mathrm{h}(t)$ within a chosen range of interest T_h as showed in Figure 2(a). In previous works, assuming the pulse heating time is T_h, then the total time interval is $T + T_h$ [24, 25]. After obtaining the coded excitation data, the output obtained by convoluting the matched filter related to the data and the coded signal is the output of ECPuCT system [26].

The basic theory of the PuC technique is presented in Figure 2(b). Given a coded excitation $\mathrm{s}(t)$ of duration T and the bandwidth B, and another signal $\psi(\mathrm{t})$, the so-called matched filter, such that their convolution "*" approximates the Dirac's Delta function $\delta(t)$ as:

$$\mathrm{s(t)} * \psi(\mathrm{t}) = \tilde{\delta}(t) \approx \delta(t) \tag{1}$$

In Eq. (1), an estimate $\tilde{h}(t)$ of the $h(t)$ is obtained by convolving the recorded output signal $\mathrm{y(t)}$ with the matched filter $\psi(t)$, the impulse response can be obtained as:

$$\begin{aligned}\tilde{h}(t) &= \mathrm{y}(t) * \psi(\mathrm{t}) = h(t) * s(t) * \psi(t) + e(t) * \psi(\mathrm{t}) \\ &= h(t) * \tilde{\delta}(t) + \tilde{e}(t) \approx h(t) + \tilde{e}(t)\end{aligned} \tag{2}$$

In Eq. (2), $s(t) * \psi(t)$ equals to the $\tilde{\delta}(t)$. One of the advantages of PuC is the impulse response can be estimated by delivering energy to the system in a long time in lower peak power compared to PT, hence it avoids possible thermal shocks in fragile materials and allowing the use of relatively-cheap heating source

such as commercial LED chips. In this way, it is possible to provide more energy, and hence to increase the SNR and detectability of eddy current thermography system. The SNR gain is proportional to the $T \times B$ product, i.e. it can be enhanced almost arbitrarily by increasing either the time duration or the bandwidth of the coded waveform. It should also be noted that the limited $T \times B$ product of practically-employed coded signals results in an $\tilde{h}(t)$ always affected by the so-called "side-lobes", i.e. any local maxima of the $\tilde{h}(t)$ amplitude except the main lobe (main peak). This can be improved by a proper choice of the matched filter signal $\psi(t)$ [27]. In this paper, s(t) is a Barker Code (BC) of order equal to 13 and the matched filter $\psi(t)$ has been chosen simply to be the time-reversed sequence of the input coded signal s(t) [28].

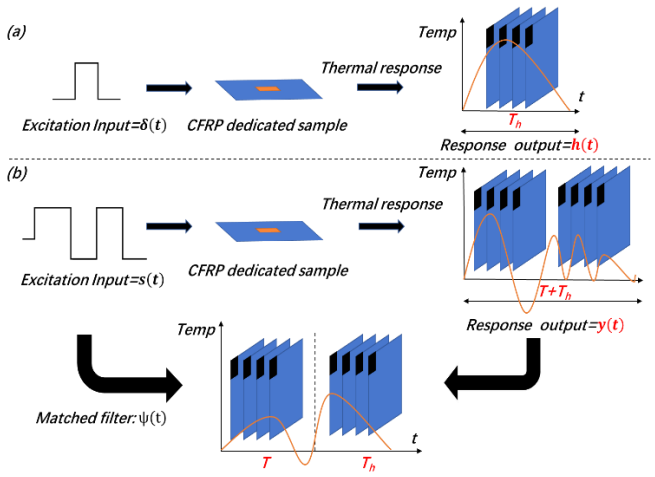

Figure 2 Estimation of impulse response: a) single pulse excitation, b) Process of impulse response calculation

B. Image PCA and impulse response PCA

The temperature distribution of surface varying with the time recorded by the IR camera, which is a 3-D thermal image sequence. In this instance, different information contained in thermal images at different time, then the thermal image sequence is a process of temperature distribution changing with time, and the amount of data is enormous. It is very inefficient to analyze temperature distribution image one by one. So, it is of considerable significance to extract the information of image sequence in time domain effectively by using a feature extraction algorithm.

Principal component analysis (PCA) is a classical statistical tool. PCA takes aim at optimal set of vector bases to represent the relationship between data. In this work, impulse response of each image in the thermal sequences regarded as independent variable in image PCA. Each extracted PC is a linear combination of the original frame. Those PCs form the basis of vector space respectively and arranged in order of decreasing variance. Therefore, the first several PCs contain the most significant information of raw data.

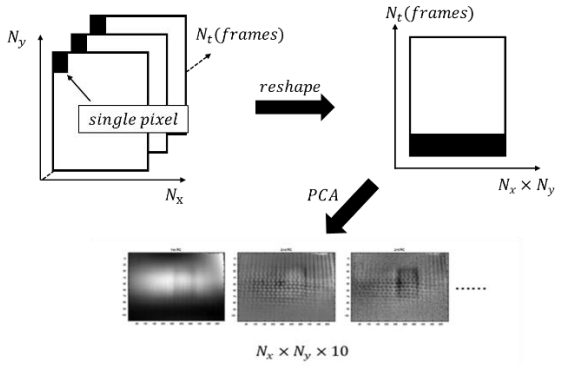

Figure 3 Diagram of image based PCA

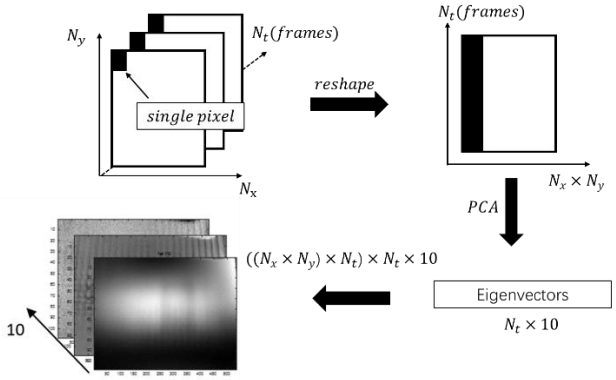

Figure 4 Diagram of impulse response based PCA

Figure 3 presents the process of image PCA. Firstly, to facilitate the use of PCA, the original 3-D data converted to a 2-D data. Then each column vector of this 2-D matrix represents the temperature curve of different positions varying with time. For image PCA, the black row represents the thermal response of a frame at one time, PCA reduces the dimensionality of data on the time axis N_t. Compared to the image PCA, impulse response PCA regards the impulse response of each pixel rather than each image in the thermal sequences. Each PC extracted from raw data represent a linear combination of the original impulse response. Figure 4 shows the diagram of impulse response PCA, a column of pixels represents the impulse response of single-pixel varying with frames (N_t).

According to the theory of ECPT system, the interaction of eddy current distribution gradually decreases as the depth of defect increases. In the heating stage, the distributions of eddy current are independent as each other, which form independent Joule heat source. Then the heat inside material is diffused along with fibre orientations. Therefore, the heat of each region interacts only with its neighbours. In the ECPT system, it is generally assumed that the heat distribution on the surface determined by the characteristic of electricity, magnetism, heat, etc. In this case, the heat distributions of two distant regions are independent of each other.

In practical progress, the surface of the sample continuously emits infrared heat radiation, and the IR camera receives the thermal radiation at time t and records the infrared thermal images $Y(t)$. Because the thermal images composed of many impulse

response pixels, these heat distributions have the same trend, which is a statistically linear correlation. The observation model $Y(t)$ expressed as follows:

$$\mathrm{Y}(t) \approx \sum_{i=1}^{N_s} m_i X_i(t) \tag{3}$$

In Eq.3, $X_i(t)$ represents the set of N_s patterns, and N_s is the number of non-linear correlated heat distributions, those patterns include defective, non-defective and other areas. m_i denotes the mixing parameters that describe the contribution of different thermal patterns to the observation output $\mathrm{Y}(t)$. To extract $X_d(t)$ that describes the defective area impulse response, kernel-PCA is applied in this work.

Based on the description of the observation model, $\mathrm{Y}(t)$ can be expressed as a combination of every pixel's impulse response:

$$\mathrm{Y}(t) = \left[X_1(t), X_2(t), X_3(t), \cdots, X_{N_x \times N_y}(t)\right] \tag{4}$$

To introduce the kernel function, the impulse response is projected to the kernel space ϕ, then the kernel matrix $\mathrm{K(i,j)}$ obtained as follows:

$$\frac{1}{N_x \cdot N_y} \sum_{i=1}^{N_x \times N_y} \left(\phi(\mathrm{X(t)} - \frac{1}{N_x \cdot N_y} \sum_{j=1}^{N_x \times N_y} \phi(\mathrm{X(t)})\right) \left(\phi(\mathrm{X(t)} - \frac{1}{N_x \cdot N_y} \sum_{j=1}^{N_x \times N_y} \phi(\mathrm{X(t)})^T\right) \tag{5}$$

In Eq.5, the Gaussian kernel function defined as:

$$\phi\big(X(t)\big) = exp\left(-\frac{\left\|\phi\big(X(t)\big) \times \phi\big(X(t)\big)^T\right\|^2}{2\sigma^2}\right) \tag{6}$$

Then the kernel matrix $\mathrm{K}(i,j)$ named as K for simple, the eigenvectors α of kernel matrix can be obtained as:

$$\lambda_i \alpha_i = K\alpha_i \tag{7}$$

Based on the obtained eigenvectors α_i, then the enhanced thermal pattern can be projected as:

$$X_d(t) = [\alpha_1, \alpha_2, \cdots \alpha_T] Y(t)^T \tag{8}$$

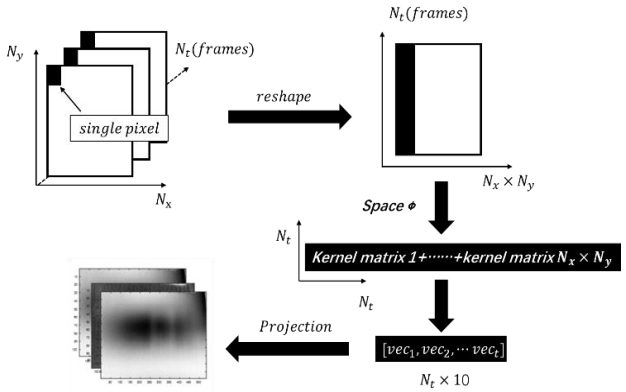

Figure 5 Diagram of K-PCA

The diagram of K-PCA presented in Figure 5, K-PCA maps the impulse response of single-pixel varying with frames (N_t) into Gaussian space, eigenvectors corresponding to the largest top ten eigenvalues selected for projection. Compared to the traditional PCA, this method processes the impulse response of each pixel rather than each image in the thermal video as an independent variable [29].

Although PCA focus on several principle components contains the thermal response, aliasing of thermal response from different regions blurred the physical meaning of the PCs, it is hard to explain those components. Because the thermal response from different regions is independent of each other, ICA can be applied in feature extraction for separation of heat distribution from different regions as far as possible. PCA is to maximize the variance, so that the residual variance is minimized, or information loss is minimal (variance is information), but ICA maximizes independence, making the joint probability closest to the component probability product [30,31].

Thermal response signal separation based on independent component analysis is a process of constantly searching for the best linear transformation [32,33]. The best linear transformation matrix finally obtained is $\widehat{W}_{ICA}$, it not only does the estimated aliasing thermal response be as independent as possible, but it also ensures that each individual component reflects a data trend. It can be expressed as follows:

$$\begin{aligned}\widehat{\mathrm{W}}_{ICA} &= \arg\max_w \prod_t \Pr(Y''(t)|W) \\ &= \arg\max_w \prod_t \prod_i \Pr\big(X_i''(t)\big)\end{aligned} \tag{9}$$

In this formula, Pr (·) represents probability density. Based on the same thermal response model (Eq.3), the diagram of ICA showed in Figure 6.

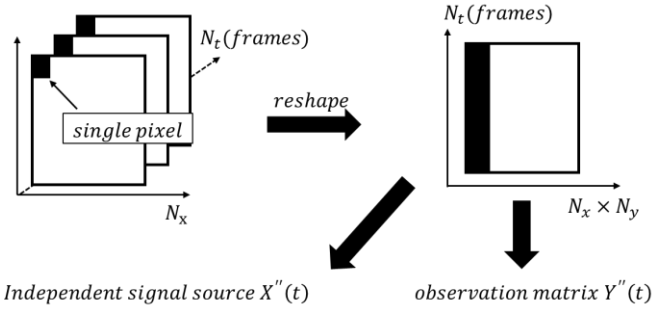

Figure 6 Diagram of ICA

In this diagram, the observation model for ICA is $Y''(t).m_i, (i = 1,2,3 \cdots N_s)$, it represents thermography image captured by the IR camera, which is considered as a mixing observation. And $X''(t)$ represents the independent signal source, it produced by position i at time t with dimensional N_s by N_y respectively. The relationship between them described in Eq.12. According to [34], $\widehat{W}_{ICA}$ can be solved with singular value decomposition. Firstly, PCA applied in whiten for $Y''(t)$, then SVD (Single value decomposition) applied, the derivation process described as follows:

$$X''(t) = \left[vec\big(X_1(t)\big), vec\big(X_2(t)\big), \cdots vec\left(X_{N_s}(t)\right)\right]^T \tag{10}$$

$$Y''(t) = \left[vec\left(Y(t)\right), vec\left(Y(t+1)\right), \cdots vec\left(Y(t+S-1)\right)\right]^T \quad (11)$$

$$Y''(t) = M_i X''(t) \quad (12)$$

$$M_i = [m_1, \cdots m_s] \quad (13)$$

$$M_1^{-1} = W \quad (14)$$

$$Y''(t)^{Nxy} = U_{N_{xy}\times N_{xy}} \times D_{N_{xy}\times N} \times V_{N\times N}^{N_{xy}} \quad (15)$$

In those formula, S represents the amount of N_{xy} represents $N_x \times N_y$, $U_{N_{xy}\times N_{xy}}, V_{N_{xy}\times N}$ are the orthogonal matrices, and $D_{N_{xy}\times N}$ contains single values. In the second stage, the independent basis vectors must be derived by employing the ICA algorithm.

$$\mathrm{U}_{N_{xy}\times N_s}^{N_{xy}} = M_{N_s\times N_s} X'_{ICA}(t) \quad (16)$$

In Eq.16, because of possible dimension reduction, e.g., choosing N_s ($N_s \leq N$) number of basis vectors informative subspace of input. $U_{N_{xy}\times N_s}$ are selected and determined by data saved in the nonzero singular values. In the end, $\widehat{\mathrm{W}}_{ICA}$ can be estimated by using a fix point iteration (FAST ICA) method.

C. Feature extraction comparison

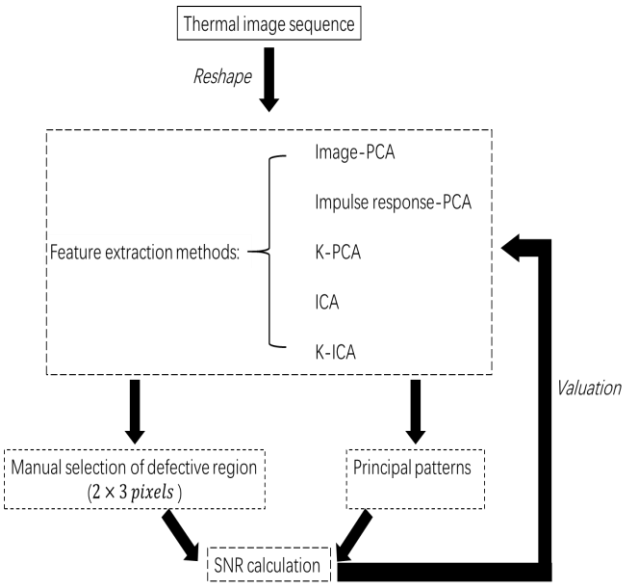

Figure 7 flowchart of SNR comparison

In this study, SNR value comparison is used to evaluate the performance of feature extraction algorithms from data [35]. This method is suitable to compare the performance of extraction algorithms in dealing with different depth defects. The value of SNR reflects the contrast between the defective area and the non-defective area, which proves which algorithms are outstanding. Considering that different pixel responses are interfered by noise in difference, manual selection of 2×3 pixels region contrasted with the sounding area. The calculation operated by the following formula:

$$\mathrm{SNR}(t) = \left|\frac{h_D(t) - \bar{h}_D(t)}{\sigma_h(t)}\right| \quad (17)$$

In Eq.17, $h_D(t)$ is the impulse response of defected area averaged over a manual selection region, $\bar{h}_D(t)$ is the impulse response averaged over whole thermal image and $\sigma_h(t)$ is the standard deviation of the manual selection region same as $h_D(t)$.

III. EXPERIMENT SETUP

A. Eddy current pulse compression thermography setup

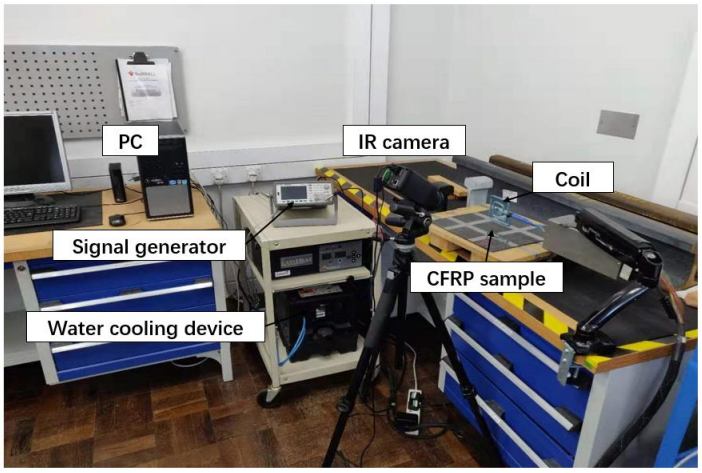

Figure 8 ECPuCT system

The system of ECPuCT that showed in Figure 8 mainly composed of a signal generator, induction heating device, excitation coil, IR camera, cooling device and PC. The signal generator sends excitation signal to the induction coil, and a trigger signal sent to the IR camera to record thermograms at 50FPS at the same time. The induction heating unit is Cheltenham EasyHeat 224, which has a maximum excitation power and current value of 2.40 kW and 400 A, respectively, and a tuneable carrier in the 150-400 kHz range. The water-cooling device is used to cool the excited coil while the coil is held 3.00mm from the sample surface to ensure that the heating of the sample is volumetric heating.

The excitation coil uses a high conductivity copper hollow control with a diameter of 6.35mm as a rectangular coil. The thermal imaging camera uses FLIR's SC7500, the thermal imager has an InSB infrared detector with a sensitive wavelength of 3-5 μm , a measurement accuracy of ±1℃ , a noise equivalent temperature difference of less than 20mK, and a resolution of 2.

B. Dedicated sample of CFRP

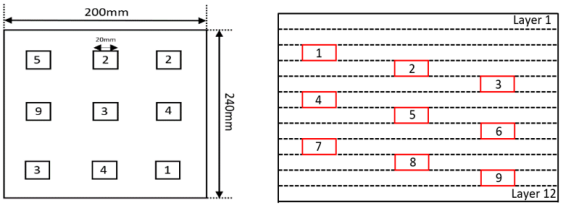

Figure 9 Plan view a) and cross-section view b)

Figure 9 shows the structure of CFRP, the dedicated sample contains twelve piles of carbon fiber fabric, the areal density is 0.2 g/*mm*3 and the fiber orientation are 0° or 90°. The lateral length is 200mm， and the width is 240mm, the total thickness of the sample is 2.80mm. The artificial delamination defects realized by inserting thin square pieces of Teflon tape. Each layer is 0.23 mm. The shallowest defect is #1 and is placed at a depth 0.46mm from the surface, the most buried defect is #9, and it placed at the depth 2.30mm.

IV. RESULTS AND DISCUSSION

A. Image PCA

As explained in section II, the image PCA algorithm is applied to extract the delamination feature and enhance the patterns. Figure 10 shows the extracted thermal patterns from original thermal sequences because carbon fibres of the sample are conductive and anisotropic; The heat produced from eddy current transfers along the direction of carbon fibres. The temperature distribution of carbon fibre structure in the defective area is abnormal, and the temperature is higher than that of carbon fibre structure in the defective region. When the delamination occurs in the carbon fibre structure, the eddy current generated will be hindered by the defects, which is equivalent to the resistance enhancement at this position. Delamination will affect the distribution of the transverse eddy current field. If the eddy current cannot flow directly through the layered position, it will bypass, which makes the delamination unable to obtain the eddy heat.

In this work, 300 frames from the 650th frame to the 949th frame as the feature extraction data, which covers the heating and cooling stage and ensures the validity of the data to the greatest extent. Every row from left to right PC1, PC2, PC3, PC4 respectively, which in turn represent the optimal 4 PCs.

The first pattern is the heating pattern that contains most information of frames, it also contains a fuzzy effect caused by transverse heat transfer, so the distribution of temperature information is vague. The second pattern clearly shows that the regular distribution of carbon fibre texture in the defective area without a fuzzy effect, which forms a sharp contrast to the carbon fibre structure is the defective area. Based on the second pattern, the location of the delamination can be determined. The third pattern shows the apparent shape of delamination as expected because it contains the essential defect information. However, it has a lower contrast between sounding area and defective area, which leads to the vague when the depth of defect becomes deeper such as #defect6 PC3.

For image PCA, the 4th pattern contains the least thermal information compared to others, so it cannot give useful information about the defect. Besides, for more profound defect, the quality of patterns become obscure, which is the reason for the introduction of impulse response PCA.

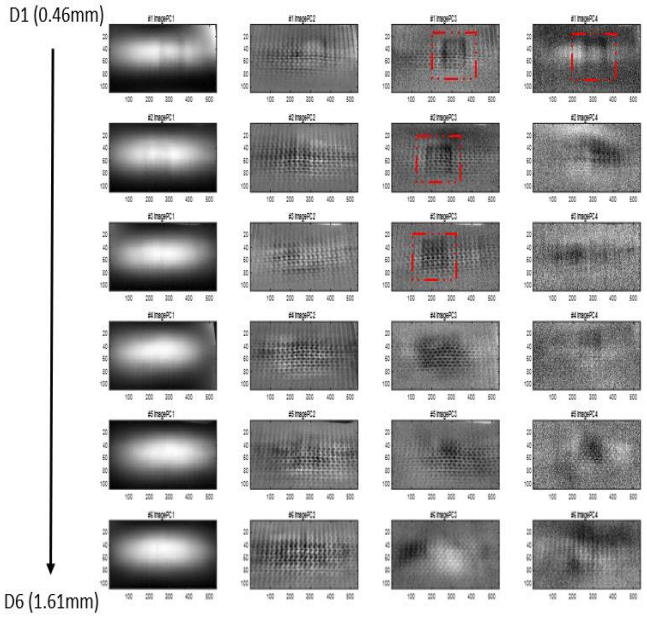

Figure 10 Results of image PCA from D1 to D6

B. Impulse response PCA

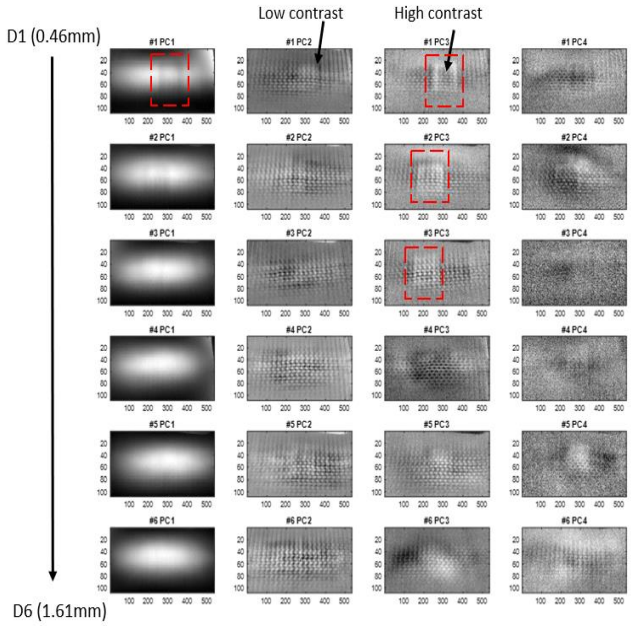

Figure 11 Results of impulse response PCA

Compared with image PCA, impulse response PCA has the advantage of feature extraction for the thermal response of each pixel, the results showed in Figure 11. For the first pattern, it is composed of plenty of thermal response information, which is reconstructed from thermal responses of pixels corresponding to the eigenvectors with the most information. There is the same problem as image PCA of PC1s, fuzzy effect leads to the image blurring so that insufficient defect information cannot be obtained. In addition, the sensitivity of PC1s is dramatically reduced when dealing with deeper defect, which of reason is 1st pattern might be cover by the heating information. 2nd pattern and 3rd pattern obtained from the second-largest eigenvector and the third-largest eigenvector; they have different contrast that marked in Figure 12.

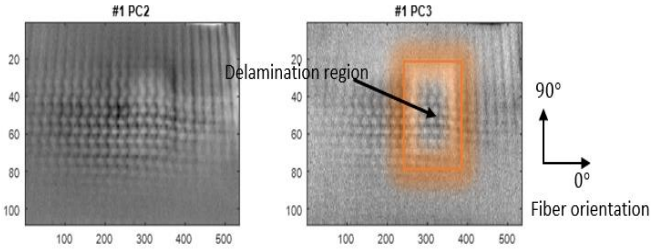

Figure 12 Contrast comparison of PC2 and PC3

The 2nd pattern shows the delamination in lower contrast while the 3rd pattern shows it in higher contrast, the reason is their corresponding eigenvectors are supposed to be orthogonal with each other. In that case, combining these two images makes it easier to determine the location, shape and size of delamination. Since the electric and thermal conductivity transfers along the fiber orientation based on sample structure, which makes the edges of delamination hotter than region of delamination. Thus, the edge has a large contrast in 1st pattern. Based on the Eq.1, the SNR of defective area heavily reduced after defect 3, the shape of delamination cannot be identified in patterns.

C. Kernel PCA

When dealing with deeper defects, the quality of thermal patterns is worse based on traditional PCA. To enhance the patterns, kernel-PCA method is applied to extract the thermal feature. According to section II, Kernel-PCA considers the impulse response of a single pixel as an independent variable, which makes the PC extracted is a linear combination of impulse responses that form the vector space respectively and arranged in order of variance reduction. Figure 13 shows the results of K-PCA.

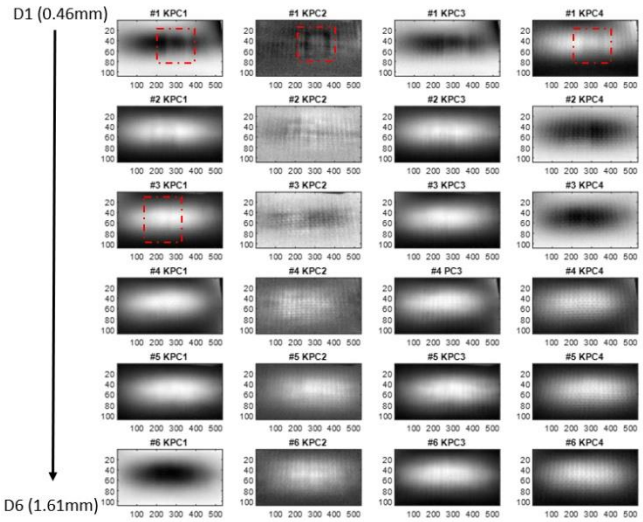

Figure 13 Results of K-PCA

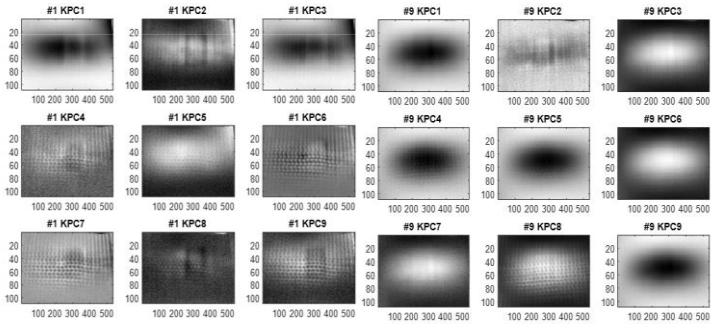

Figure 14 Comparisons of defect#1 and defect#9

In Figure 14, patterns after 4th show the edges of delamination because the eigenvectors corresponding to the first few PCs contain too much heat information. In addition, the kernel-PCA cannot arrange order of eigenvectors before projection, thus the patterns arranged as random. Another improvement of K-PCA is noise immunity when dealing with deepest defect#9, the edges of delamination presented in the second pattern.

D. ICA and kernel ICA

Independent component analysis was applied in this work to extract the features and separate the thermal distribution from different regions. The results showed in Figure 16.

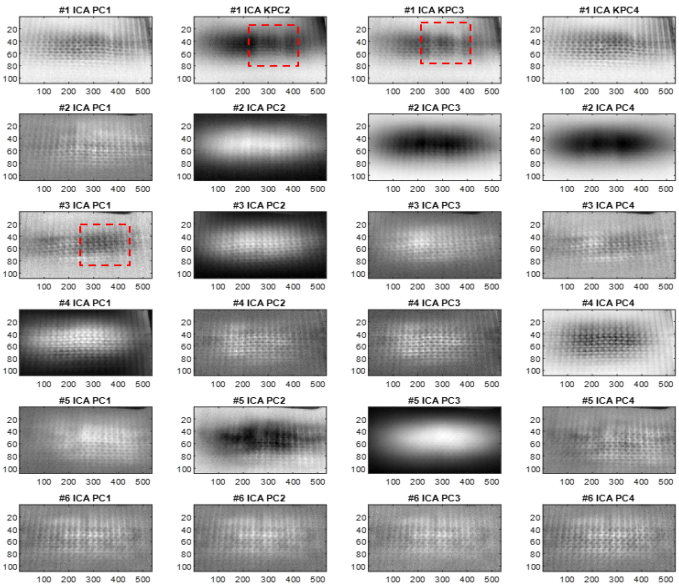

Figure 16 Results of ICA

Because ICA considers the separation of thermal distribution of impulse responses, thermal response along the fiber orientations preserved in patterns. For the same reason, the contrast of the second patterns and third patterns increases based on the ICA method. In the first patterns reconstructed by the first independent components, non-uniform heating along the coil can be eliminated. While in 4th patterns reconstructed by the fourth independent component, the edges and location of delamination can be found. Based on the patters of defect#1 to defect#6, the contrast between defective and non-defective regions is obviously higher than that of PCA methods. Therefore, the ICA based on image construction method can be used to reduce the effect of non-uniform heating, enhance the delamination detectability, and separate the thermal responses.

The preponderance of the ICA algorithm embodies in dealing with deep defect such as defect#9, the results of defect#9 showed in Figure 15. Most of those patterns can show the contrast of delamination region and non-defective area, which is better than the results of PCA provide before. However, there is a fly in the ointment that the edges of delamination can be present in most of those patterns. To tackle this challenge, ICA combined with the kernel function proposed in the work. Because the distribution of impulse responses corresponding to the Gaussian distribution, Gaussian kernel introduced in the work. The results showed in Figure 17.

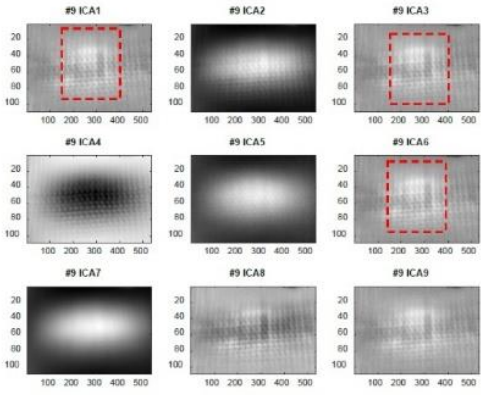

Figure 15 Patterns of defect#9 based on ICA

Combining with mesh figure of the second pattern of defect#1 based on PCA and K-ICA, ICA with kernel function is significantly to improve the contrast between defective and non-defective regions. Although the texture of carbon fibre showed clearly than other methods mentioned before, the edges of delamination are not shown in patterns.

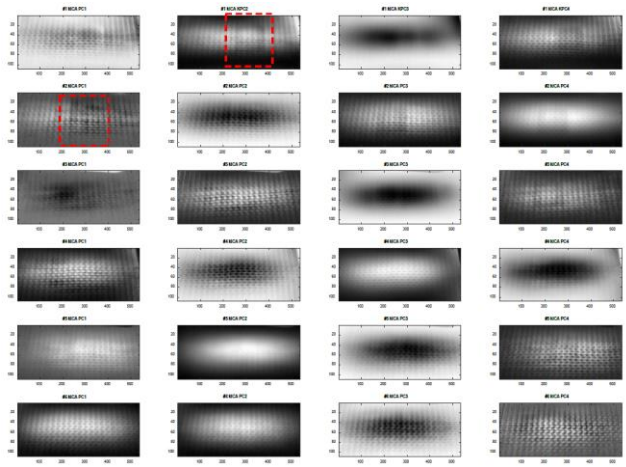

Figure 17 Results of kernel ICA

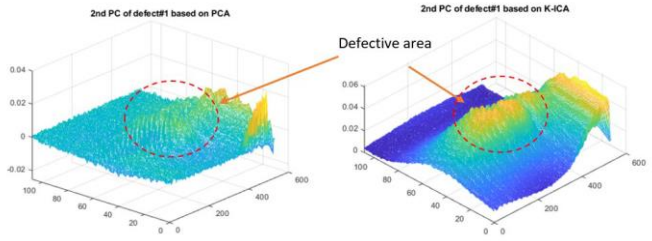

Figure 18 Mesh figure comparison of PCA and K-ICA

After comparison experiments, the patterns corresponding to the first ten independent components affected by the fuzzy effect and heating information. Because Kernel-ICA separates most of the thermal responses come from heating information and background noise, so the range of independent components should

be expanded approximately. In this work, the first twenty independent components are selected, and the delamination is concentrated from 13th frame to 15th frame. In additional, K-PCA also performs better than ICA extracting deeper defect feature.

This section discussed the results of the feature extraction. In terms of pattern quality, the quality of K-PCA presents more of the edges of delamination, and the results of ICA show more contrast between the defective area and the non-defective area. Both of PCA and ICA, they do not need to make a specific assumption of the source signal, the PCA considers that the most of useful information for a random signal included in the variance, the ICA aims at the separation of independent components composed thermal information and defect information. Therefore, their results highlight different details. In order to compare the advantages and disadvantages of these methods, the next section presents the comparison of SNR value to evaluate their performance.

E. Features comparison

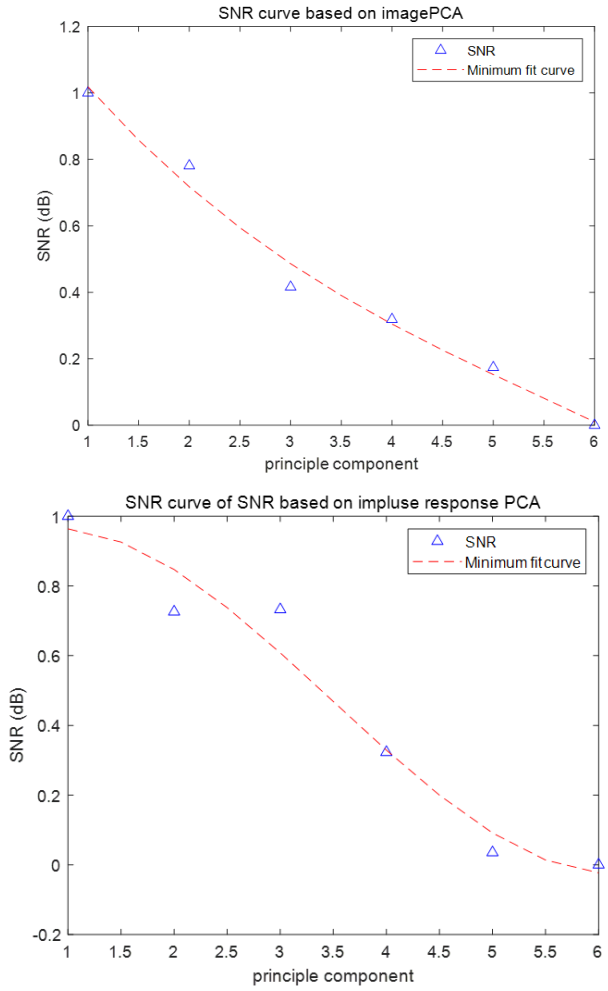

Figure 19 SNR comparison of image based PCA and impulse response based PCA

In

Figure , the SNR of image PCA is linear and monotonic decline, which is accorded with the theory of image PCA. Despite some errors and noise effects, the SNR of the defects corresponding to the six principal components decreases with the increase of depth. Because impulse response PCA focus on the instantaneous thermal response of a single pixel, the data are distributed nonlinearly. The decline rate of impulse response PCA is obviously slower than that of image PCA when dealing with deep defects. Therefore, impulse response PCA is more reliable than image PCA method.

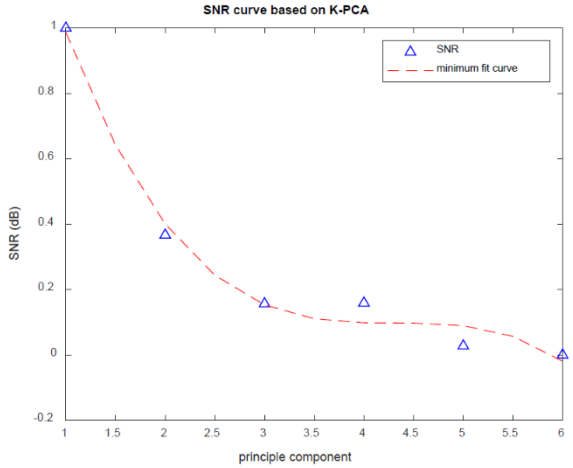

Figure 20 SNR of K-PCA

In Figure 20**,** the SNR of K-PCA declines rapidly between defect#1 and defec#2, which indicates that the heating information contained in the principal component is reduced heavily. After the second point, the decrease of information corresponding to the principal component becomes gentle, most of SNRs are concentrated in the range from 0 to 0.1. The results also prove that when the data mapped into Gauss space, the data become separable linearly. Therefore, most of the heating information that affect detection is filtered out. Combining with the results of K-

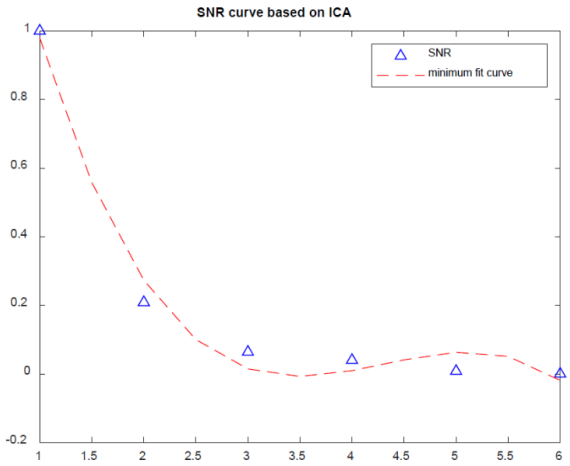

Figure 19 SNR of ICA

PCA, K-PCA performs better than traditional PCA in detecting delamination of CFRP in practice.

Due to the skin-effect, the eddy current density decayed exponentially, which reflected in the SNR curve of ICA. In Figure 19, there is a slight difference between ICA curve and K-PCA curve, which indicates that ICA does not improve image quality. According to the ICA theory, ICA capable of the separation of independent components and screen out the most differential components for image reconstruction. Therefore, the patterns of ICA reflect the differences between individual thermal responses, but SNR values not improved.

V. CONCLUSION

In this work, feature extraction techniques of impulse response have been exploited in terms of principal component analysis (PCA), kernel principal component analysis (K-PCA) and independent component analysis (ICA) The conclusion is as follows:

1. Traditional PCA has the advantage of simple implementation and fast calculation speed. However, the limitations of PCA are obvious, such as it can solve the linear correlation well, but there is no way for high-order correlation.
2. For data possess high-order correlation, kernel PCA is worth considering because the nonlinear correlation is converted to linear correlation by kernel function. Since the thermal response distribution is consistent with a Gaussian distribution, Kernel-PCA with Gaussian kernel adopted in this work. However, K-PCA and PCA affected by non-uniform heating pattern.
3. Because of the independence and non-correlation between thermal responses, ICA was applied in feature extraction. Compared with PCA methods, ICA performs better when dealing with deep defect.

According to the properties of SNR curve, the performance of K-PCA is the most stable and corresponds to the corresponding physical phenomena. Eddy current density exponential decays with the depth increases, which corresponds to the SNR curve of K-PCA is exponential.

Based on the drawbacks discussed before, the future work will investigate:

1. Extracting the complex defect feature and evaluating the method performance.

2. The next step is to analyze the lateral diffusion of heat and minimize its impact on the experimental results.

VI. ACKNOWLEDGEMENT

The authors would like to thank Hamed Malekmohammadi from University of Perugia for his contribution to the experimental study and the sample provided. This paper is funded by the European Union's Horizon 2020 research and innovation programme under the Marie Skłodowska-Curie grant agreement No 722134 – NDTonAIR.

VII. REFERENCES

[1] J. Wilson, G. Tian, I. Abidin, S. Yang, and D. Almond, "Pulsed eddy current thermography: system development and evaluation," *Insight-Non-Destructive Testing and Condition Monitoring*, vol. 52, no. 2, pp. 87-90, 2010.

[2] Y. He, G. Tian, M. Pan, and D. Chen, "Impact evaluation in carbon fiber reinforced plastic (CFRP) laminates using eddy current pulsed thermography," *Composite Structures*, vol. 109, pp. 1-7, 2014.

[3] Z. P. Liu, X. Li, M. C. Li, X. L. Liu, and L. Ke, "Research of Detecting Methods of Welding Cracks in CFRP-Steel Structures Based on Eddy Current Pulsed Thermography," in *Materials Science Forum*, 2016, vol. 860: Trans Tech Publ, pp. 53-56.

[4] V. Revol, B. Plank, R. Kaufmann, J. Kastner, C. Kottler, and A. Neels, "Laminate fibre structure characterisation of carbon fibre-reinforced polymers by X-ray scatter dark field imaging with a grating interferometer," *NDT & E International*, vol. 58, pp. 64-71, 2013.

[5] N. Akhter, H. C. Jung, H.-S. Chang, and K.-S. Kim, "Location of delamination in laminated composite plates by pulsed laser holography," *Optics and Lasers in Engineering*, vol. 47, no. 5, pp. 584-588, 2009.

[6] H. D. Benítez, C. Ibarra-Castanedo, A. Bendada, X. Maldague, H. Loaiza, and E. Caicedo, "Definition of a new thermal contrast and pulse correction for defect quantification in pulsed thermography," *Infrared Physics & Technology*, vol. 51, no. 3, pp. 160-167, 2008.

[7] X. Maldague, "Theory and practice of infrared technology for nondestructive testing," 2001.

[8] F. Ciampa, P. Mahmoodi, F. Pinto, and M. Meo, "Recent advances in active infrared thermography for non-destructive testing of aerospace components," *Sensors*, vol. 18, no. 2, p. 609, 2018.

[9] C. Gao, W. Q. Meeker, and D. Mayton, "Detecting cracks in aircraft engine fan blades using vibrothermography nondestructive evaluation," *Reliability Engineering & System Safety*, vol. 131, pp. 229-235, 2014.

[10] L. Cheng, B. Gao, G. Y. Tian, W. L. Woo, and G. Berthiau, "Impact damage detection and identification using eddy current pulsed thermography through integration of PCA and ICA," *IEEE Sensors Journal*, vol. 14, no. 5, pp. 1655-1663, 2014.

[11] P. Zhu, L. Bai, Y. Cheng, and C. Yin, "Selection of significant independent components in eddy current pulsed thermography non-destructive testing," in *2015 IEEE International Instrumentation and Measurement Technology Conference (I2MTC) Proceedings*, 2015: IEEE, pp. 853-857.

[12] L. Bai, B. Gao, G. Y. Tian, W. L. Woo, and Y. Cheng, "Spatial and time patterns extraction of eddy current pulsed thermography using blind source separation," *IEEE sensors Journal*, vol. 13, no. 6, pp. 2094-2101, 2013.

[13] H. Yang, B. Gao, G. Tian, W. Ren, and W. L. Woo, "Transient-spatial pattern mining of eddy current pulsed thermography using wavelet transform," *Chinese Journal of Mechanical Engineering*, vol. 27, no. 4, pp. 768-778, 2014.

[14] Q. Yi, G. Tian, H. Malekmohammadi, J. Zhu, S. Laureti, and M. Ricci, "New features for delamination depth evaluation in carbon fiber reinforced plastic materials using eddy current pulse-compression thermography," *NDT & E International*, vol. 102, pp. 264-273, 2019.

[15] N. Tabatabaei and A. Mandelis, "Thermal-wave radar: A novel subsurface imaging modality with extended depth-resolution dynamic range," *Review of Scientific Instruments*, vol. 80, no. 3, p. 034902, 2009.

[16] R. Mulaveesala, J. S. Vaddi, and P. Singh, "Pulse compression approach to infrared nondestructive characterization," *Review of Scientific Instruments*, vol. 79, no. 9, p. 094901, 2008.

[17] R. Mulaveesala and S. Venkata Ghali, "Coded excitation for infrared non-destructive testing of carbon fiber reinforced plastics," *Review of Scientific Instruments*, vol. 82, no. 5, p. 054902, 2011.

[18] G. Tian, A. Sophian, D. Taylor, and J. Rudlin, "Wavelet-based PCA defect classification and quantification for pulsed eddy current NDT," *IEE Proceedings-Science, Measurement and Technology*, vol. 152, no. 4, pp. 141-148, 2005.

[19] M. Pan, Y. He, G. Tian, D. Chen, and F. Luo, "Defect characterisation using pulsed eddy current thermography under transmission mode and NDT applications," *Ndt & E International*, vol. 52, pp. 28-36, 2012.

[20] B. Gao, L. Bai, W. L. Woo, G. Y. Tian, and Y. Cheng, "Automatic defect identification of eddy current pulsed thermography using single channel blind source separation," *IEEE Transactions on Instrumentation and Measurement*, vol. 63, no. 4, pp. 913-922, 2013.

[21] J. Liu, W. Yang, and J. Dai, "Research on thermal wave processing of lock-in thermography based on analyzing image sequences for NDT," *Infrared Physics & Technology*, vol. 53, no. 5, pp. 348-357, 2010.

[22] L. Jingxiang and G. Liu, "Noise reduction in magneto-acousto-electrical NDT using analytic wavelet thresholding," in *2017 IEEE 3rd Information*

Technology and Mechatronics Engineering Conference (ITOEC), 2017: IEEE, pp. 585-588.

[23] Y. Wang, B. Gao, G. Tian, W. L. Woo, and Y. Miao, "Diffusion and separation mechanism of transient electromagnetic and thermal fields," *International Journal of Thermal Sciences*, vol. 102, pp. 308-318, 2016.

[24] G. Tian, Y. Gao, K. Li, Y. Wang, B. Gao, and Y. He, "Eddy current pulsed thermography with different excitation configurations for metallic material and defect characterization," *Sensors*, vol. 16, no. 6, p. 843, 2016.

[25] Y. Gao *et al.*, "Electromagnetic pulsed thermography for natural cracks inspection," *Scientific reports*, vol. 7, p. 42073, 2017.

[26] X. Li, Z. Liu, X. Jiang, and G. Lodewijks, "Method for detecting damage in carbon-fibre reinforced plastic-steel structures based on eddy current pulsed thermography," *Nondestructive Testing and Evaluation*, vol. 33, no. 1, pp. 1-19, 2018.

[27] G. Riegert, T. Zweschper, and G. Busse, "Lockin thermography with eddy current excitation," *Quantitative InfraRed Thermography Journal*, vol. 1, no. 1, pp. 21-32, 2004.

[28] G. Silipigni *et al.*, "Optimization of the pulse-compression technique applied to the infrared thermography nondestructive evaluation," *NDT & E International*, vol. 87, pp. 100-110, 2017.

[29] J. Gong, J. Liu, L. Qin, and Y. Wang, "Investigation of carbon fiber reinforced polymer (CFRP) sheet with subsurface defects inspection using thermal-wave radar imaging (TWRI) based on the multi-transform technique," *Ndt & E International*, vol. 62, pp. 130-136, 2014.

[30] S. Laureti, G. Silipigni, L. Senni, R. Tomasello, P. Burrascano, and M. Ricci, "Comparative study between linear and non-linear frequency-modulated pulse-compression thermography," *Applied optics*, vol. 57, no. 18, pp. D32-D39, 2018.

[31] S. Laureti *et al.*, "The use of pulse-compression thermography for detecting defects in paintings," *NDT & E International*, vol. 98, pp. 147-154, 2018.

[32] C. Xu, N. Zhou, J. Xie, X. Gong, G. Chen, and G. Song, "Investigation on eddy current pulsed thermography to detect hidden cracks on corroded metal surface," *NDT & E International*, vol. 84, pp. 27-35, 2016.

[33] G. N. Costache, P. Corcoran, and P. Puslecki, "Combining PCA-based datasets without retraining of the basis vector set," *Pattern Recognition Letters*, vol. 30, no. 16, pp. 1441-1447, 2009.

[34] G. Mayr, G. Stockner, H. Plasser, G. Hendorfer, and P. Burgholzer, "Parameter estimation from pulsed thermography data using the virtual wave concept," *NDT & E International*, vol. 100, pp. 101-107, 2018.

[35] R. Yang and Y. He, "Eddy current pulsed phase thermography considering volumetric induction heating for delamination evaluation in carbon fiber reinforced polymers," *Applied Physics Letters*, vol. 106, no. 23, p. 234103, 2015.